MAGNETOHYDRODYNAMICS Vol. 00 (1964), No. 00, pp. 1–??

# Dynamo action in cellular convection

*N. Seehafer*[1], *A. Demircan*[2]

[1] *Institut für Physik, Universität Potsdam, PF 601553, 14415 Potsdam, Germany*
[2] *Weierstraß-Institut für Angewandte Analysis und Stochastik, Mohrenstr. 39, 10117 Berlin, Germany*

The dynamo properties of square patterns in Boussinesq Rayleigh-Bénard convection in a plane horizontal layer are studied numerically. Cases without rotation and with weak rotation about a vertical axis are considered, particular attention being paid to the relation between dynamo action and the kinetic helicity of the flow. While the fluid layer is symmetric with respect to up-down reflections, the square-pattern solutions may or may not possess this vertical symmetry. Vertically symmetric solutions, appearing in the form of checkerboard patterns, do not possess a net kinetic helicity and we find them to be incapable of dynamo action at least up to magnetic Reynolds numbers of $\approx 12000$. Vertically asymmetric squares, a secondary convection pattern appearing via the skewed varicose instability of rolls and being characterized by rising (descending) motion in the centers and descending (rising) motion near the boundaries, can in turn be devided into such that possess full horizontal square symmetry and others lacking also this symmetry. The flows lacking both the vertical and horizontal symmetries are particularly interesting in that they possess kinetic helicity and show kinematic dynamo action even without rotation. The generated magnetic fields are concentrated in vertically oriented filamentary structures near cell boundaries. The dynamos found in the nonrotating case are, however, always only kinematic, never nonlinear dynamos. Nonlinearly the back-reaction of the magnetic field then forces the flow into the basin of attraction of a roll-pattern solution incapable of dynamo action. But with rotation added parameter regions are found where a subtle balance between the Coriolis and Lorentz forces enables nonlinear dynamo action of stationary asymmetric squares. In some parameter regions this balance leads to nonlinear dynamos with flows in the form of oscillating squares or stationary modulated rolls.

**Introduction** Studies of convection-driven dynamos have concentrated either on turbulent convection [1] or on convection near onset, where simple steady flows can be obtained [2, 3, 4, 5]. In this paper we report on the dynamo properties of convection in the simple form of squares (see also [6, 7, 8]).

The typical convective patterns are different for convection with up-down reflection symmetry and such lacking this symmetry, where symmetry of the convection means symmetry of the governing equations and boundary conditions for the deviations of the physical quantities from their values in the nonconvective state. Rayleigh-Bénard Boussinesq convection with symmetric top and bottom boundary conditions possesses the up-down reflection symmetry, and its preferred convection pattern near onset is rolls, i.e. the convective pattern is also up-down symmetric. However, recently it was found both experimentally and theoretically that other, *vertically asymmetric* states, namely convection in the form of squares or hexagons, can coexist with the roll states in a parameter range where only rolls were previously known to be stable [6, 9, 10, 11]. These asymmetric squares and hexagons, with rising or with descending motion in the center (and descending or rising motion near the boundary) are usually observed in convection lacking up-down reflection symmetry, namely in compressible convection [12, 13], in fluids with strongly temperature dependent viscosity [14] or in Bénard-Marangoni convection [15, 16]. The vertically asymmetric square pattern represents the dom-

inating pattern over a wide range of the control parameters both in vertically symmetric and nonsymmetric convection. Details about this type of convection are found in [6, 11, 17]. In the present paper we deal with squares in Boussinesq, i.e. vertically symmetric convection. Here besides the vertically asymmtric square patterns also vertically symmetric ones are found, which appear in the form of checkerboard patterns. However, with respect to the dynamo effect the asymmetric squares turn out to be much more interesting than the symmetric ones.

It is well known that a nonvanishing kinetic helicity, for a given volume $V$ defined by $H = \int_V \mathbf{v}\cdot\nabla\times\mathbf{v}\,\mathrm{d}^3\mathbf{x}$, where $\mathbf{v}$ denotes the fluid velocity and $h = \mathbf{v}\cdot\nabla\times\mathbf{v}$ is the helicity density, is favorable at least for the large-scale dynamo action of small-scale velocity fields [18]. We pay particular attention to the relation between dynamo action and the kinetic helicity of the underlying flows.

**1. Equations and parameters** We consider buoyancy-driven rotating convection in an electrically conducting plane fluid layer heated from below. Using the Oberbeck-Boussinesq approximation, the governing system of partial differential equations reads as follows:

$$\nabla\cdot\mathbf{v} = 0 \tag{1}$$

$$\frac{\partial\mathbf{v}}{\partial t} + (\mathbf{v}\cdot\nabla)\mathbf{v} = -\nabla p + P\,\nabla^2\mathbf{v} + PR\,\theta\mathbf{e}_z + (\nabla\times\mathbf{B})\times\mathbf{B} + P\sqrt{T}\,\mathbf{v}\times\mathbf{e}_z \tag{2}$$

$$\nabla\cdot\mathbf{B} = 0 \tag{3}$$

$$\frac{\partial\mathbf{B}}{\partial t} + (\mathbf{v}\cdot\nabla)\mathbf{B} = PP_m^{-1}\nabla^2\mathbf{B} + (\mathbf{B}\cdot\nabla)\mathbf{v} \tag{4}$$

$$\frac{\partial\theta}{\partial t} + \mathbf{v}\cdot\nabla\theta = v_z + \nabla^2\theta\,. \tag{5}$$

Equations (1)–(5) are given in usual dimensionless form. $\mathbf{B}$ is the magnetic field and $p$ and $\theta$ represent the deviations of pressure and temperature from their values in the pure conduction state. We use Cartesian coordinates $x$, $y$ and $z$ with the $z$ axis in the vertical direction antiparallel to the gravitational force. $\mathbf{e}_z$ is the unit vector in the vertical direction. There are four dimensionless parameters, the Prandtl number $P$, the magnetic Prandtl number $P_m$, the Rayleigh number $R$ and the Taylor number $T$, defined by

$$P = \frac{\nu}{\kappa}, \qquad P_m = \frac{\nu}{\eta}, \qquad R = \frac{\alpha g d^3}{\nu\kappa}\delta T, \qquad T = \left(\frac{2\Omega d^2}{\nu}\right)^2, \tag{6}$$

where $\nu$ is the kinematic viscosity, $\kappa$ the thermal diffusivity, $\eta$ the magnetic diffusivity, $\alpha$ the volumetric expansion coefficient, $g$ the gravitational acceleration, $d$ the thickness of the fluid layer, $\delta T$ the temperature difference between the upper and lower boundaries and $\Omega$ the angular velocity of the rotation. $R$ measures the strength of the buoyancy forces and $T$ the rotation rate. We apply periodic boundary conditions with spatial period $L$ in the horizontal directions $x$ and $y$. The top and bottom planes are assumed to be stress-free, isothermal and impenetrable for matter and electromagnetic energy:

$$\frac{\partial v_x}{\partial z} = \frac{\partial v_y}{\partial z} = v_z = \theta = \frac{\partial B_x}{\partial z} = \frac{\partial B_y}{\partial z} = B_z = 0 \quad \text{at } z = 0, 1 \tag{7}$$

As in [6, 19, 20] we restrict ourselves to the case of a vanishing mean horizontal flow since such a flow can be removed by a Galilean transformation. In our

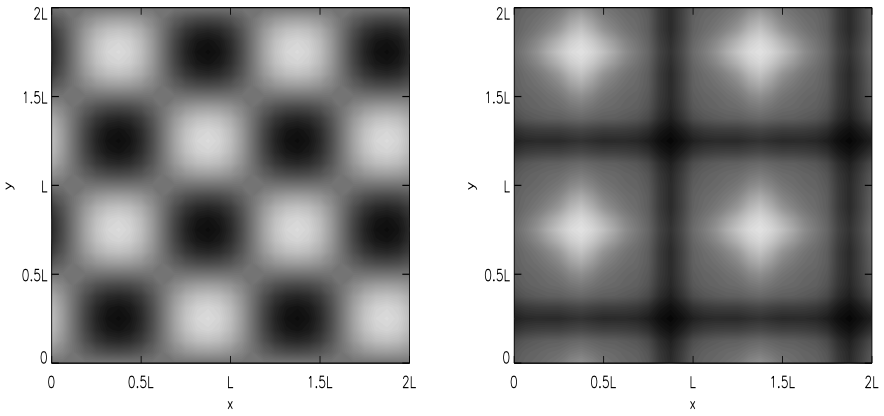


(a) (b)

Figure 1: Shadowgraph images of the vertical velocity component $v_z$ in the horizontal midplane for $T = 0$. Bright areas refer to positive values where the motion of the fluid is upwards. (a) Unstable checkerboard pattern for $R = 1000$, (b) stable asymmetric square pattern for $R = 7000$.

numerics we used a pseudospectral method with a spatial resolution of $32^3$ points for simulations and $16^3$ points for non-simulative eigenvalue and eigenvector calculations. The main results were checked by additional simulations at a resolution of $64 \times 64 \times 16$. The aspect ratio is kept fixed at $L = 4$ for the dynamo calculations; but in preceding purely hydrodynamic calculations of the underlying convective patterns also $L$ was varied. The Prandtl number is 6.8 and the Taylor number is restricted to values below the critical one for the Küppers-Lortz [21] instability, i.e. the instability of convection rolls with respect to other rolls rotated by a certain angle relative to the original rolls, which results in a dynamics dominated by heteroclinic cycles formed by unstable roll states and connections between them [20, 22]); dynamo action in rapidly rotating convection is studied in [23, 24].

**2. Convection in the form of squares** Without rotation, flows in the form of vertically symmetric squares or checkerboard patterns could only be observed as transient phenomena (but see Sec. 3.1 for the case with rotation). By contrast, vertically asymmetric squares were found as stable stationary attractors. Examples of convection in the form of vertically symmetric and asymmetric squares in the absence of rotation are shown in Fig. 1. The asymmetric squares [Fig. 1(b)] are a secondary convection pattern and appear via the skewed-varicose instability [25] of primary convection rolls. Results of a stability analysis are shown in Fig. 2; for more details we refer to [6].

Depending on the initial conditions, cells with rising or descending motion in the center appear. The spectrum of the excited Fourier modes shows that the vertically asymmetric squares can be represented to lowest order by

$$\left(A_1 e^{i\mathbf{k_1 x}} + A_2 e^{i\mathbf{k_2 x}}\right) + \left(B_1 e^{i(\mathbf{k_1}+\mathbf{k_2})\mathbf{x}} + B_2 e^{i(\mathbf{k_1}-\mathbf{k_2})\mathbf{x}}\right) + c.c. \qquad (8)$$

where $\mathbf{k_1}$ and $\mathbf{k_2}$ are horizontal wave vectors given by $\mathbf{k_1} = (0, k)$ and $\mathbf{k_2} = (k, 0)$.

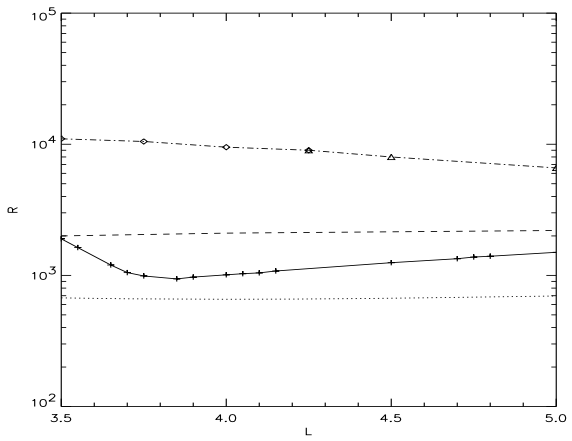


Figure 2: The region of stable squares in the $L$-$R$ plane. The dashed line specifies the skewed varicose instability for rolls and indicates the transition from a roll pattern to a square pattern for increasing Rayleigh number. The back transition from the squares to the rolls for decreasing $R$ is shown by the solid line, with + signs marking the calculated points. The dashed-dotted line indicates instability of the squares for increasing $R$, diamonds denoting a double Hopf bifurcation and triangles a single Hopf bifurcation. For reference, the linear stability boundary of the nonconvective ground state to rolls is shown by the dotted line.

$k$ is the fundamental wave number of the asymmetric squares. $A_1 \exp(i\mathbf{k_1 x})$ and $A_2 \exp(i\mathbf{k_2 x})$ represent two rolls with the same wave number $k$, one parallel to the $x$ axis and the other parallel to the $y$ axis, while the two terms with coefficients $B_1$ and $B_2$, respectively, correspond to rolls parallel to the diagonals of the periodicity square, perpendicular to each other and with the same wave number $q = |\mathbf{k_1} + \mathbf{k_2}| = \sqrt{2}k$, which is the wave number of the skewed-varicose unstable rolls (the instability thus leads to a pattern with a smaller wave number). For asymmetric squares as shown in Fig. 1(b) to appear it is essential that all four wave vectors $\mathbf{k_1}$, $\mathbf{k_2}$, $\mathbf{k_1} + \mathbf{k_2}$ and $\mathbf{k_1} - \mathbf{k_2}$ are excited [i.e. all four coefficients $A_1$, $A_2$, $B_1$ and $B_2$ in Eq. (8) must be different from zero]. The wave numbers $k$ and $q$ are in resonance through triadic interactions of these wave vectors [26]. A representation like Eq. (8) was used in [17] to study square cells in non-Boussinesq convection near onset and is contained in a more general Galerkin ansatz used in [11] to study asymmetric squares in Boussinesq convection. Asymmetric squares were also found numerically in compressible magnetoconvection near onset [12]. A major difference between the checkerboard and vertically asymmetric square solutions is that the latter ones require the excitation of two different wave numbers ($k$ and $q$) and their nonlinear resonance, while the checkerboards are "linear" squares with only one wave number excited.

Without rotation, the checkerboard-pattern solutions are symmetric to reflections in vertical planes parallel to one of the sides or diagonals of a square. The symmetry to reflections in vertical planes implies zero net helicity (since helicity is a pseudoscalar and thus changes sign under reflections). We find the checkerboard-pattern solutions to be always unstable in the nonrotating case. In the same case, i.e. for $T = 0$, the vertically asymmetric square solutions may or may not possess horizontal $D_4$ symmetry; the dihedral group $D_4$ contains all rotations and reflections which transform a square in a plane into itself. We find that these

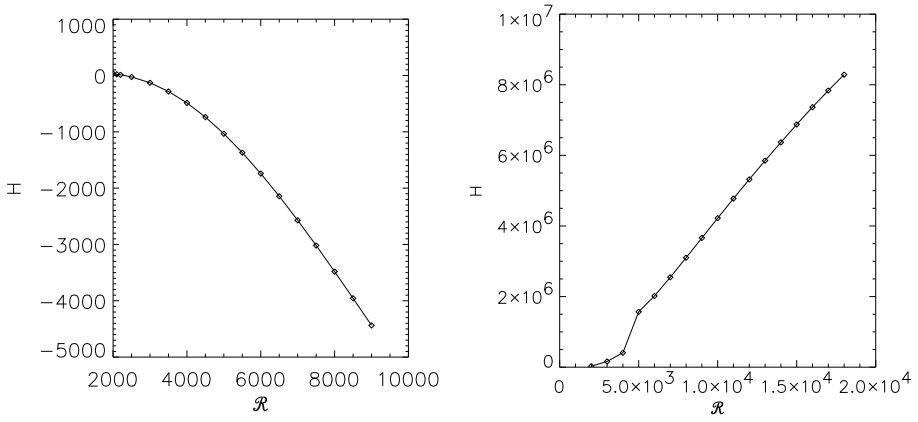


(a) (b)

Figure 3: The helicity of an upflow square as a function of the Rayleigh number for (a) $T = 0$ and (b) $T = 100$.

symmetries are either all present (for the $D_4$ symmetric solutions) or all broken (for the solutions without the $D_4$ symmetry). For the $D_4$ symmetric solutions one has $A_1 = A_2$ and $B_1 = B_2$ in Eq. (8). Like for the checkerboard-pattern solutions, the symmetry to reflections in vertical planes then implies zero net helicity.

For the vertically asymmetric solutions lacking the horizontal $D_4$ symmetry at $T = 0$, there is no reflection symmetry that would prohibit a nonzero net helicity, and such a net helicity is indeed found: Fig. 3(a) shows the helicity of a nonrotating upflow square as a function of the Rayleigh number in the range where the flow is stationary. The solutions possess a net helicity even in the absence of rotation. If rotation at low rates about the vertical axis is added, the pattern is modified but still corresponds to asymmetric squares. Compared to the case without rotation, the stability boundary towards higher values of $R$, where the pattern loses stability to oscillatory solutions [6], is shifted upwards. In Fig. 3(b) the helicity as a function of the Rayleigh number for a case with rotation ($T = 100$) is shown. The helicity due to rotation is significantly larger than the "self-helicity" of the nonrotating squares already for very low rotation rates. In addition, stable rotating squares can be traced to higher values of the Rayleigh number where the helicity is by several orders of magnitude larger than for the nonrotating squares.

## 3. Dynamo action in square convection

*3.1. Kinematic dynamo* Our primary convection solutions are stationary and correspond either to rolls or to checkerboard patterns. Checkerboard patterns are observed for Taylor numbers around 225 [20]. The primary roll and checkerboard-pattern solutions were checked for kinematic dynamo action in the (small) Rayleigh number interval close to the onset of convection where they are stable ($R \approx 1000 \ldots 2000$). The checkerboard-pattern solutions were additionally checked in the regions close to the onset of convection where they are unstable but the roll solutions are stable — they were then constructed as superpositions

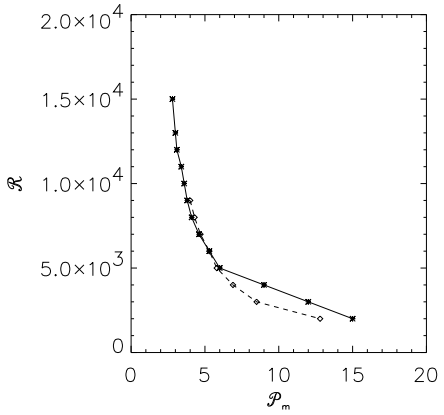


Figure 4: Stability boundary for the kinematic dynamo instability in the $P_m$-$R$ plane. The dashed line corresponds to the nonrotating case and the continuous line to $T = 100$.

of two solutions corresponding to rolls with the same wave number and axes perpendicular to each other. The net helicity in the periodic box vanishes for both types of solutions, even if $T \neq 0$ [although for $T \neq 0$ each single roll or square (vertical upflow or downflow column with square cross section) has a nonvanishing helicity]. We always find the two primary convection states to be incapable of kinematic dynamo action. The kinematic dynamo properties of the two flows were determined up to magnetic Prandtl numbers $P_m = 5000$; the associated magnetic Reynolds numbers then increase to values $R_m \approx 12000$. No kinematic dynamo action was found. Similarly, we find the vertically asymmetric-square solutions with horizontal $D_4$ symmetry (existing only in the absence of rotation) to be incapable of kinematic dynamo action. This was tested for magnetic Reynolds numbers up to $R_m \approx 13000$ (at $R = 8000$ we have a flow for which $R_m \approx 13000$ if $P_m \approx 100$).

The convection flows in the form of vertically asymmetric squares without horizontal $D_4$ symmetry, however, can act as kinematic dynamos even without rotation. In Fig. 4 results for the nonrotating case and for $T = 100$ are given. The two curves in the $P_m$-$R$ plane are stability boundaries where a single real eigenvalue becomes positive and the kinematic dynamo starts. The magnitude of the helicity does not seem to be the most crucial factor for the onset of the kinematic dynamo, though after onset the dynamo growth rates increase much faster with $R$ if rotation is present. For small Rayleigh numbers, $R <\approx 5000$, the dynamo sets in at lower values for the magnetic Prandtl number without rotation than with rotation. This can be explained by the fact that with rotation the convection is still very weak here since rotation increases the critical Rayleigh number for the onset of convection.

An example of the magnetic field generated by kinematic dynamo action is depicted in Fig. 5. The field is concentrated in filamentary structures which are aligned along the vertical axis and situated close to cell boundaries of the velocity field.

*3.2. Nonlinear dynamo* Fig. 6(a) shows the time evolutions of magnetic and kinetic energies starting from a square pattern velocity field and a small seed magnetic field for the case without rotation. Initially the magnetic field grows

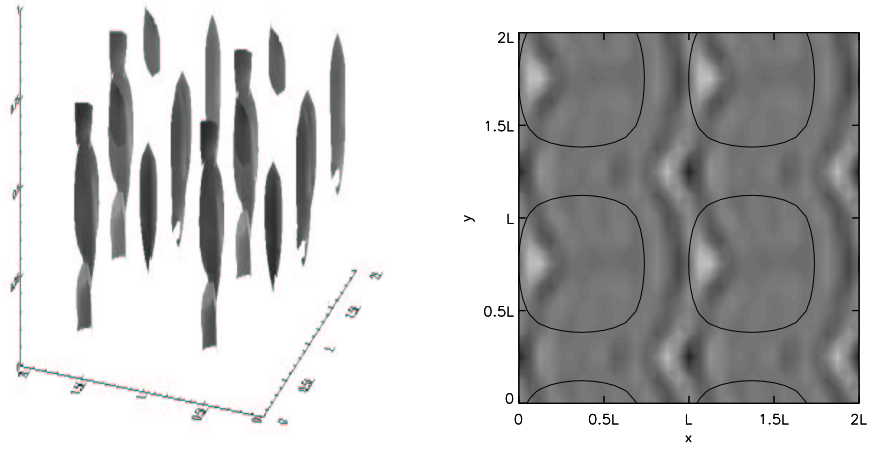


(a) (b)

Figure 5: Unstable magnetic eigenmode for the velocity field shown in Fig. 1(b) and $P_m = 5.5$. (a) Isosurface of the magnetic field strength at 50% of the peak field. (b) Shadowgraph image of the vertical component $B_z$ in the horizontal midplane, bright areas indicating positive values; in addition the null line of the vertical velocity component $v_z$ in the midplane is shown.

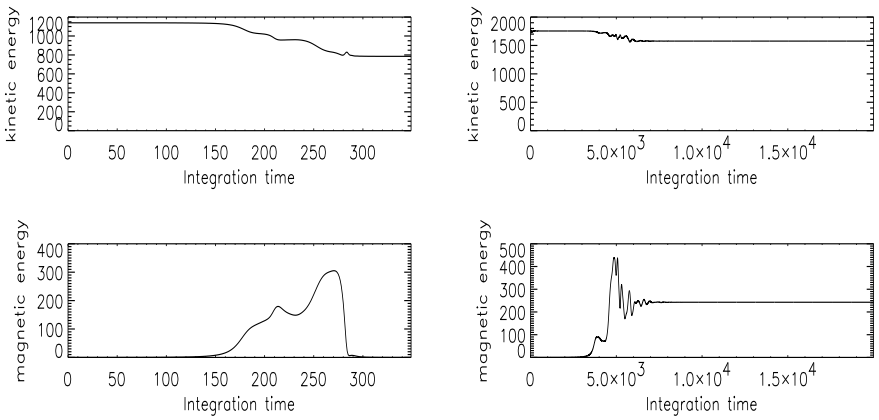


(a) (b)

Figure 6: Time evolutions of kinetic and magnetic energies for (a) $T = 0$, $R = 5000$ and $P_m = 6$ and (b) $T = 10$, $R = 7000$ and $P_m = 4.65$. Time is measured in units of the thermal diffusion time.

exponentially with a well defined growth rate. In this kinematic phase the Lorentz force is negligible and the square pattern remains undisturbed. However, after the magnetic perturbation has reached a strength suffcient to influence the flow, it forces the solution into the basin of attraction of the two-dimensional roll state with wave number $k$. The roll solution is incapable of dynamo action and the magnetic field decays to zero. This effect of self-extinguishing of the dynamo by the back-reaction of the magnetic field was recently also observed for flow in triply periodic Cartesian geometry driven by an explicit forcing [27], spherical dynamo models with rotation and explicit forcing [28] and two-dimensional convection rolls in a plane layer rotating about an oblique axis [5].

That is to say, in the nonrotating case the asymmetric squares are only kinematic, not nonlinear dynamos. Nonlinear dynamo action is only possible if additional effects are included that counteract the self-extinguishing of the dynamo by the Lorentz force. We add background rotation at very low rates, namely $0 \leq T \leq 150$. For these small Taylor numbers the asymmetric square solutions are hydrodynamically stable, that is to say, the nonrotating squares can be continued on a stable solution branch towards higher Taylor numbers. Although the mechanism behind the self-extinguishing is still acting, there are parameter ranges where a nonlinear dynamo is found. Time evolutions of kinetic and magnetic energies in such a case, with $T = 10$, $R = 7000$ and $P_m = 4.65$, are given in Fig. 6(b). After the initial kinematic phase, a back reaction of the magnetic field is clearly visible. But though the velocity field is modified, it still corresponds to an asymmetric square pattern. The magnetic field saturates and is maintained for all time.

It seems that for our system and in the parameter range studied, nonlinear dynamo action requires a subtle balance between the Coriolis and Lorentz forces. A similar balance between these two forces characterizes the weak-field limit of the Childress-Soward dynamo [2, 29], which however works in a *rapidly* rotating convective layer. Plus symbols (+) in Fig. 7 mark the parameter range in the $T$-$P_m$ plane where we observe nonlinear dynamos with underlying stationary asymmetric square patterns. The Rayleigh number is fixed at $R = 7000$. By simultaneously varying $T$ (i.e the strength of the Coriolis force) and $P_m$ (i.e. the strength of the Lorentz force) we also find magnetic attractors which differ from the stationary squares. The additional types of magnetic attractors are oscillating squares [indicated by diamonds ($\Diamond$) in Fig. 7] and stationary rolls [indicated by triangles ($\triangle$) in Fig. 7]. The stationary magnetic rolls show a modulation along the roll axis and disappear if the magnetic field is switched off. The solution then falls back on the simple roll state (without modulation) with wave number $k$, which is not capable of kinematic dynamo action. In the non-marked regions of the $P_m$-$T$ plane self-extinguishing leads to nonmagnetic final states.

Our investigations were focused on small Taylor numbers $T < 150$. For higher Taylor numbers the convection is governed by alternating rolls [20] and we observe dynamo properties similar to those found in [24].

An interesting question is whether there exist nonvanishing horizontal averages $\mathbf{B}_h$ of the dynamo-generated magnetic fields since these correspond to large-scale fields. We find that always

$$\mathbf{B}_h(z) = \int_{\text{periodicity box}} \mathbf{B}\, \mathrm{d}x\mathrm{d}y \neq \mathbf{0}\,. \tag{9}$$

This indicates that our small-scale dynamos are mean-field or large-scale dynamos as well.

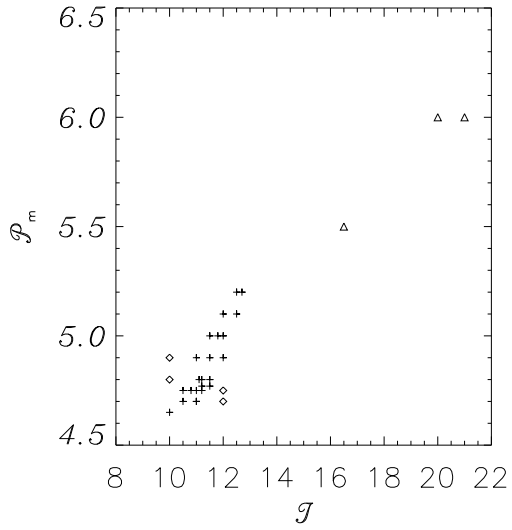


Figure 7: Parameter range of nonlinear dynamo action in the $T$-$P_m$ plane for $R = 7000$. Plus symbols (+) refer to dynamos with flows in the form of stationary asymmetric squares. Dynamos in oscillating squares are denoted by diamonds ($\Diamond$) and such in stationary rolls by triangles ($\triangle$).

**4. Conclusion** We have studied the dynamo properties of square patterns in nonrotating and weakly rotating Boussinesq Rayleigh-Benard convection in a plane horizontal layer. Vertically symmetric solutions appear in the form of checkerboard patterns. They do not possess a net kinetic helicity and we find them to be incabable of dynamo action (at least up to magnetic Reynolds numbers of $\approx 12000$). Square-pattern solutions lacking the vertical symmetry are characterized by rising (descending) motions in the centers and descending (rising) motion near the boundaries of the squares. As a secondary convection pattern they appear via the skewed varicose instability of rolls and can in turn be divided into solutions with the full horizontal $D_4$ symmetry of a square and others lacking also this symmetry (with rotation added the horizontal $D_4$ symmetry is always broken). The solutions lacking both the vertical and the $D_4$ symmetries possess kinetic helicity and show kinematic dynamo action even without rotation. The generated magnetic fields are concentrated in vertically oriented filamentary structures near cell boundaries. The dynamos found in the nonrotating case are, however, always only kinematic, never nonlinear dynamos. Nonlinearly the back-reaction of the magnetic field then forces the flow into the basin of attraction of a roll-pattern solution incapable of dynamo action. But with rotation added parameter regions are found where stationary asymmetric squares are also nonlinear dynamos. These nonlinear dynamos are seemingly characterized by a subtle balance between the Coriolis and Lorentz forces. In some parameter regions this balance also leads to nonlinear dynamos with flows in the form of oscillating squares or stationary modulated rolls.

**Acknowledgements** Figures 1(a,b), 3(a,b), 4 and 6(a,b) were first published in [7] and are shown here with kind permission of Kluwer Academic Publish-

ers. Figures 5(a,b) and 7 were published in [8] and are shown with kind permission of Taylor & Francis Ltd.

## REFERENCES


1. A. Brandenburg, et al. Magnetic structures in a dynamo simulation. *J. Fluid Mech.*, vol. 306 (1996), pp. 325–352.
2. A. M. Soward. A convection-driven dynamo I. The weak field case. *Phil. Trans. R. Soc. London A*, vol. 275 (1974), pp. 611–646.
3. Y. Fautrelle and S. Childress. Convective dynamos with intermediate and strong fields. *Geophys. Astrophys. Fluid Dynam.*, vol. 22 (1982), pp. 235–279.
4. V. A. Zheligovsky and D. J. Galloway. Dynamo action in Christopherson hexagonal flow. *Geophys. Astrophys. Fluid Dynam.*, vol. 88 (1998), pp. 277–293.
5. P. C. Matthews. Dynamo action in simple convective flows. *Proc. R. Soc. London A*, vol. 455 (1999), pp. 1829–1840.
6. A. Demircan and N. Seehafer. Nonlinear square patterns in Rayleigh-Bénard convection. *Europhys. Lett.*, vol. 53 (2001), pp. 202–208.
7. A. Demircan and N. Seehafer. Dynamos in rotating and nonrotating convection in the form of asymmetric squares. In P. Chossat, D. Armbruster, and I. Oprea, editors, *Dynamo and Dynamics, a Mathematical Challenge* (Kluwer, Dordrecht, 2001), pp. 163–171.
8. A. Demircan and N. Seehafer. Dynamo in asymmetric square convection. *Geophys. Astrophys. Fluid Dynam.*, vol. 96 (2002), pp. 461–479.
9. M. Assenheimer and V. Steinberg. Observation of coexisting upflow and downflow hexagons in Boussinesq Rayleigh-Bénard convection. *Phys. Rev. Lett.*, vol. 76 (1996), pp. 756–759.
10. R. M. Clever and F. H. Busse. Hexagonal convection cells under conditions of vertical symmetry. *Phys. Rev. E*, vol. 53 (1996), pp. R2037–R2040.
11. F. H. Busse and R. M. Clever. Asymmetric squares as an attracting set in Rayleigh-Bénard convection. *Phys. Rev. Lett.*, vol. 81 (1998), pp. 341–344.
12. P. C. Matthews, M. R. E. Proctor, and N. O. Weiss. Compressible magnetoconvection in three dimensions: planforms and nonlinear behaviour. *J. Fluid Mech.*, vol. 305 (1995), pp. 281–305.
13. A. M. Rucklidge, et al. Compressible magnetoconvection in three dimensions: pattern formation in a strongly stratified layer. *J. Fluid Mech.*, vol. 419 (2000), pp. 283–323.
14. D. S. Oliver and J. R. Booker. Planform of convection with strongly temperature-dependent viscosity. *Geophys. Astrophys. Fluid Dynam.*, vol. 27 (1983), pp. 73–85.
15. K. Eckert, M. Bestehorn, and A. Thess. Square cells in surface-tension-driven Bénard convection: experiment and theory. *J. Fluid Mech.*, vol. 356 (1998), pp. 155–197.
16. M. F. Schatz, et al. Time-independent square patterns in surface-tension-driven Bénard convection. *Phys. Fluids*, vol. 11 (1999), pp. 2577–2582.
17. M. R. E. Proctor and P. C. Matthews. $\sqrt{2}$ : 1 resonance in non-Boussinesq convection. *Physica D*, vol. 97 (1996), pp. 229–241.
18. F. Krause and K.-H. Rädler. *Mean-Field Magnetohydrodynamics and Dynamo Theory* (Akademie-Verlag, Berlin, 1980).
19. S. Scheel and N. Seehafer. Bifurcation to oscillations in three-dimensional Rayleigh-Bénard convection. *Phys. Rev. E*, vol. 56 (1997), pp. 5511–5516.

20. A. Demircan, S. Scheel, and N. Seehafer. Heteroclinic behavior in rotating Rayleigh-Bénard convection. *Eur. Phys. J. B*, vol. 13 (2000), pp. 765–775.

21. G. Küppers and D. Lortz. Transition from laminar convection to thermal turbulence in a rotating fluid layer. *J. Fluid Mech.*, vol. 35 (1969), pp. 609–620.

22. F. H. Busse and K. E. Heikes. Convection in a rotating layer: A simple case for turbulence. *Science*, vol. 208 (1980), pp. 173–175.

23. M. G. St. Pierre. The strong field branch of the Childress-Soward dynamo. In M. R. E. Proctor, P. C. Matthews, and A. M. Rucklidge, editors, *Theory of Solar and Planetary Dynamos* (Cambridge University Press, Cambridge, 1993) pp. 295–302.

24. C. A. Jones and P. H. Roberts. Convection-driven dynamos in a rotating plane layer. *J. Fluid Mech.*, vol. 404 (2000), pp. 311–343.

25. F. H. Busse and R. M. Clever. Instabilities of convection rolls in a fluid of moderate Prandtl number. *J. Fluid Mech.*, vol. 91 (1979), pp. 319–335.

26. M. Silber and A. C. Skeldon. Parametrically excited surface waves: Two-frequency forcing, normal form symmetries, and pattern selection. *Phys. Rev. E*, vol. 59 (1999), pp. 5446–5456.

27. N. H. Brummell, F. Cattaneo, and S. M. Tobias. Linear and nonlinear dynamo action. *Phys. Lett. A*, vol. 249 (1998), pp. 437–442.

28. H. Fuchs, K.-H. Rädler, and M. Rheinhardt. On self-killing and self-creating dynamos. *Astron. Nachr.*, vol. 320 (1999), pp. 129–133.

29. S. Childress and A. M. Soward. Convection driven hydromagnetic dynamo. *Phys. Rev. Lett.*, vol. 29 (1972), pp. 837–839.